ARITHMETIC METHODS
IN MATHEMATICAL PHYSICS AND BIOLOGY
BANACH CENTER PUBLICATIONS, VOLUME 109
INSTITUTE OF MATHEMATICS
POLISH ACADEMY OF SCIENCES
WARSZAWA 2016

A NUMERICAL METHOD TO DIFFERENTIATE BETWEEN "PURE" AND "IMPURE" FRACTALS

MARTIN OBERT, MAILIN TIEFENBACH, GUNHILD MARTELS

Department of Diagnostic and Interventional Radiology, University Hospital Giessen
Justus-Liebig-University Giessen, Klinikstrasse 33, 35392 Giessen, Germany
E-mail: martin.obert@radiol.med.uni-Giessen.de

BARBARA AHLEMEYER

Institute for Anatomy and Cell Biology, Division of Medical Cell Biology II
Justus-Liebig-University Giessen, Aulweg 123, 35392 Giessen, Germany

GABRIELE A. KROMBACH and MARIAN KAMPSCHULTE

Department of Diagnostic and Interventional Radiology, University Hospital Giessen
Justus-Liebig-University Giessen, Klinikstrasse 33, 35392 Giessen, Germany

Abstract. We introduce a numerical method that enables the differentiation between natural fractal image representations of objects that have only fractal properties ("pure" fractals) from those that have partial Euclidean and partial fractal properties ("impure" fractals). We evaluate our classification method on a numerically constructed fractal that serves as "pure" fractal and compare it with an "impure" digital image representation of the blood vessel system of a mouse-liver. Our classification method is based on the study of the invariance of a data set under different levels of image-data-point reductions — comparing a dissection and a random erosion method. The various image-sets were characterized by the fractal dimension D, evaluated by the mass radius method. The differentiation between "pure" and "impure" fractals is performed by their different and opposite behavior when the reduction is performed at average reduction levels: We find for the "pure" fractal that dissections lead to no D-difference between complete and reduced sets; contrary, the erosion method leads to a noticeable D-difference. These findings swap for the "impure" fractal. Here we find that dissections lead to distinct D-differences between complete and reduced sets; contrary, the erosion method leads to no change in these D-differences. We assume that this differentiation can be applied successfully when automated image classifications are desired or necessary.

2010 *Mathematics Subject Classification*: Primary 92B99; Secondary 92-08.
Key words and phrases: "pure" and "impure" fractals, mass radius analysis, image analysis, automatic image classification, micro Computed Tomography.
The paper is in final form and no version of it will be published elsewhere.

DOI: 10.4064/bc109-0-9

1. Introduction. In the context of image analysis of natural irregular sets, the fractal concept of geometry [M] plays a fundamental role. It enables a well-defined numerical characterization of complex, heterogeneous, and disordered sets in terms of the fractal dimension. An adequate lingual description is often impossible or at least very difficult. Some sets have the property that their entire system is fractal. The numerical construction of a Sierpiński triangle can serve as image-example, which is calculated up to a certain iteration level during the recursive image generation [S]. We call such a system "pure" fractal. On the other side, many natural objects of our special interest may contain subsets that can be described in parts as fractals, in parts as Euclidean shaped systems [MRR]. The radiological obtained digital image data set of the blood vessel system of a mouse-liver can serve as an example. Individual vessels have the appearance of a tube. A tube has an Euclidean shaped two-dimensional surface and an Euclidean shaped three-dimensional volume. On the other hand, the complete liver vessel-system is a tube network, made up of many branches, which is a fractal. Hence, the blood vessel set consists of a mixed geometry that we call "impure" fractal. It is therefore desirable to be able to differentiate between such "pure" and "impure" fractals, since differentiations are the basics of classifications in general. One can differentiate between these sets just by visual inspection. Thus, in times where automated image analysis is gaining more and more importance, we want to find a well-defined numerical method that can help to perform the classification.

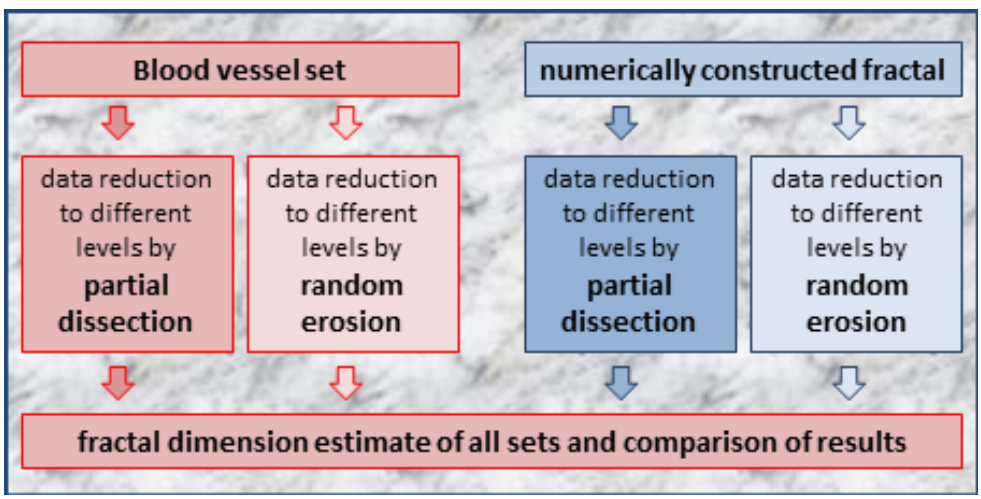

Fig. 1. Flowchart of the investigation's workflow

To accomplish this, we investigate numerically the invariance of a digital image set under dissection and under erosion. Dissection is defined as an operation that breaks a complete object into smaller parts. A dissection example would be to cut an apple into two pieces. Erosion is defined as operation that removes tiny parts of a complete object at randomly chosen positions. An erosion example would be the dissolution process of a metal sponge that is put in a vessel with acid, where some metal parts are solved at arbitrarily positions of the sponge. Both data reduction methods imply the diminishing of points or voxels that make up the digital image representation of vessels or particles

in the real world. Note that particle reduction always leads to a point-size reduction of a set. Particle reduction must not necessarily imply a spatial size reduction, which leads to a smaller diameter of an object.

We use D to characterize the irregularity of the complete and the reduced sets [M, PO]. The mass radius method is used to numerically estimate D [O, SJJ, AL]. D of the "pure" and "impure" fractals is studied for both reduction methods as function of data reduction.

Fig. 1 gives an overview over the general workflow and the image-sets that are investigated in this study.

2. Materials and methods. In this section we describe the origin of the scanned mouse-liver, the preparation of the studied blood vessel system and its filling with contrast agent, the radiological imaging method, the image reconstruction method, the vessel segmentation, the subset dissection, and how the random-erosion is conducted. We then describe the numerical construction of the fractal curve, the subset dissection method, and the random erosion method. Finally, we describe the mass radius analysis.

2.1. Origin of the digital image-data of the mouse. A digital data set of a liver from a healthy mouse was obtained from an animal experiment performed in the Department of Diagnostic and Interventional Radiology that was completely unrelated to this study. All experiments from that investigation were approved by the local governmental authorities and performed according to the guidelines for animal protection.

A healthy mouse was sacrificed. Next, the left ventricle of the heart was punctured for a systemic perfusion with 10 ml heparin-saline solution followed by perfusion with 10 ml Microfil® (MV-122, FlowTech, Carver, MA, USA). Systemic perfusion leads to a filling of the liver blood vessels via the arteria hepatica propria and the vena portae. We call the space filled with Microfil for shortness "blood vessel system" or "vessel system". Microfil is a lead-containing liquid plastic that hardens approximately two hours after injection and that produces high x-ray attenuation in a Computed Tomography scan. This leads to a visual enhancement of contrast of the perfused vessels compared to the surrounding soft tissue of the liver. The liver of the mouse was excised and positioned on the specimen holder of the used CT-system.

2.2. Radiological data acquisition and image reconstruction. Imaging was performed with a micro-Computed Tomography (μCT), Skyscan® 1072, Bruker microCT, Kontich, Belgium. Scans were performed at 80 kVp (tube voltage) and 100 μA (tube current). The radiation time for the liver scan was 2.5 hours. The field of view of this μCT is not large enough to investigate the complete mouse-liver. Therefore, only a part of the liver was imaged. The exact anatomical position of the dissected part is not described in further detail.

The μCT's raw data were reconstructed with a cone-beam filtered back-projection algorithm into a $768 \times 403 \times 616$ voxel matrix, where 768×403 is the xy-matrix-size of the reconstructed DICOM-image stack. The 616 indicates the complete image number in z-direction of the liver scan. The size of the scanned volume is $15.36 \times 8.06 \times 12.32$ mm^3. The isotropic voxels have the border size 0.020 mm.

The reconstructed image data were transferred to a Windows Vista operated PC with a 3 GHz Intel®Core™ 2 Duo CPU and 6 GB of RAM. This computer was used for the numerical image analysis in this investigation.

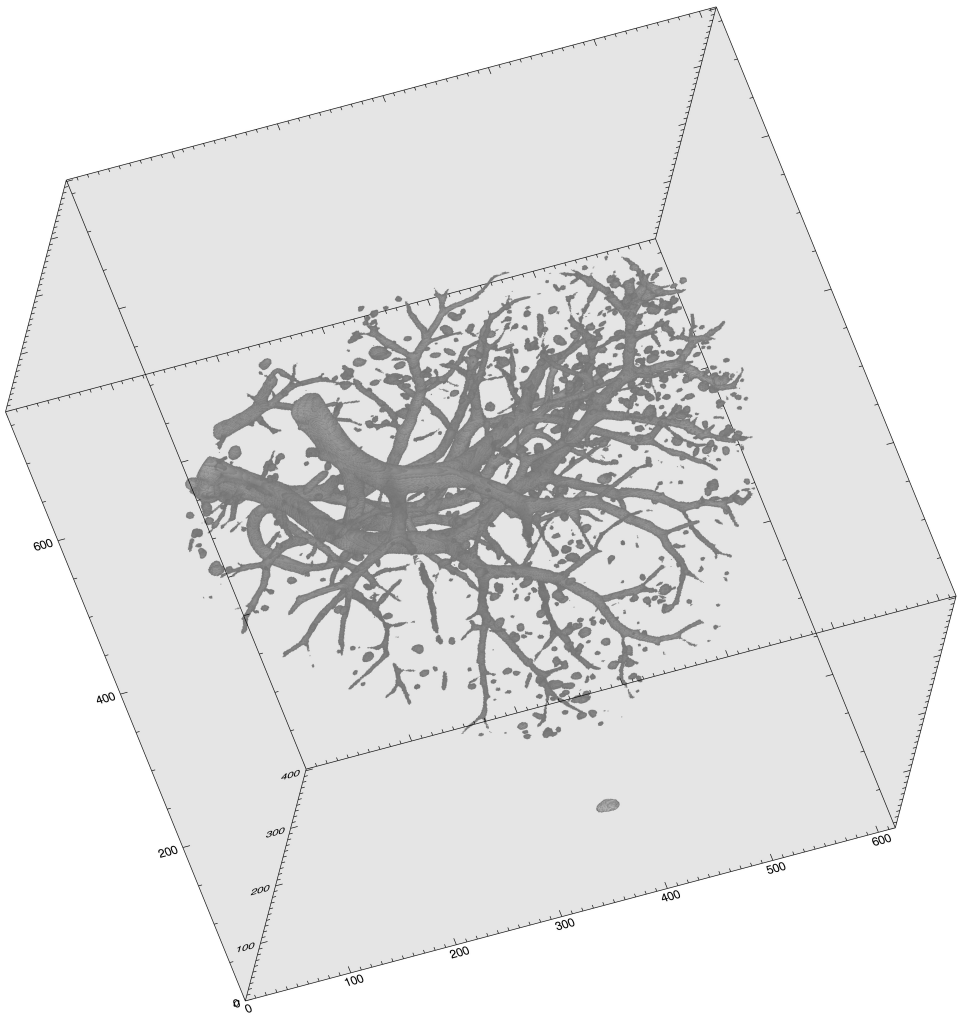

Fig. 2. Volume rendering image of the binary blood vessel system of a part of a mouse-liver obtained by μCT. The image visualizes a segmentation result of a grey-level range being larger than 130 grey-level units in the original radiological data set. The suboptimal visualization of small vessels, which is caused by incomplete and inconsistent Microfil® perfusion, is completely irrelevant in this investigation

2.3. Blood vessel segmentation. The μCT's grey level values in the range from 0 to 255 are related to the x-ray attenuation. Zero corresponds to air and 255 to the structures with the highest x-ray attenuation on a linear scale. Blood vessel segmentation was performed by a threshold, which selects all voxels in the mouse-liver data set that have a grey level larger than 130. This value ensures that only parts of the vessel system and no parts of soft liver tissue are segmented. Next, the data set is transformed into

binary data where all selected vessel-voxels are set to 1, and all other voxels are attributed a value of 0. The sum of all vessel-voxels gives the number of data points of the complete liver vessel set. We call this number n_{liver}, which is 958,792. The segmentation result of the liver vessels is shown in Fig. 2. All voxel's xyz-coordinates of the segmented vessel-system are written to a computer disk, so that they are available for further numerical evaluations.

We now describe the data reduction method that leads to dissected subsets. To obtain a dissected subset, images are deleted from the beginning or from the end of the image data stack in different orders of magnitude. As example, the complete liver data stack is found in the z-image range from $[0, 618]$. A smaller set is obtained, if e.g. the first 100 images of the set are dissected or cut out, so that the resulting set contains only the z-image range from e.g. $[100, 618]$. Since the set is irregular and inhomogeneous, the number of vessel voxels or points within a dissected image-range cannot be predicted in advance. Numerous dissected subsets are generated that contain 0.46, 0.82, 0.89, 1.65, 3.13, 6.04, 6.30, 12.74, 13.09, 21.71, 25.10, 28.71, 38.64, 49.60, 67.00, 75.28, 80.68, 90.24, and 96.59 percent voxels of the complete vessel-voxel set.

We now describe the data reduction method that lead to eroded subsets. We wrote a computer program that performs the following steps: At first, the list of data points of the complete vessel-voxel set was read into the memory of the computer. Each data point of the list contains a voxel's xyz-coordinates. Next, a random number generator is used to generate two different random numbers in the range between 0 and $n_{\text{liver}} - 1$, which are interpreted as positions of the xyz-coordinates in the vessel-voxel list. After that, the coordinates of the corresponding positions of the random numbers are exchanged. This process of coordinate-position exchange is repeated 5,000,000 times and the result is stored in a new list. The described shuffling process ensures that no information of previous neighborhood-voxels of the original voxel list is preserved in the newly generated list. This method allows that an arbitrary number of points m can be read from the beginning of the shuffled new voxel list, that can be interpreted as an eroded subset of the complete vessel set, when m is smaller than n_{liver}. Since n_{liver} is known, it is trivial to produce sets that contain a chosen number of m points that correspond to a desired reduction rate of the complete set. We generated the following reduced eroded data sets that contain 0.098, 0.195, 0.39, 0.78, 1.56, 3.13, 6.25, 12.5, 21.0, 25.0, 28.0, 38.0, 50.0, 67.0, 75.0, 80.0, and 90.0 percent voxels of the complete blood vessel set.

2.4. Generation of a constructed fractal and description of the method to produce dissected and eroded subsets. The numerically constructed set in Fig. 3 shows the sixth iteration of a fractal curve that is generated by an iterative procedure as it is described in Mandelbrot [M, page 144] for the Menger sponge. We used a closed cube as initiator, a generator with $N = 11$ segments, and a reduction factor $r = 1/3$. Hence,

$$D = \frac{\ln N}{\ln(1/r)} \sim 2.1827.$$

N^6, which is 1,771,561, is the number of points in the numerical approximation of our investigated fractal set.

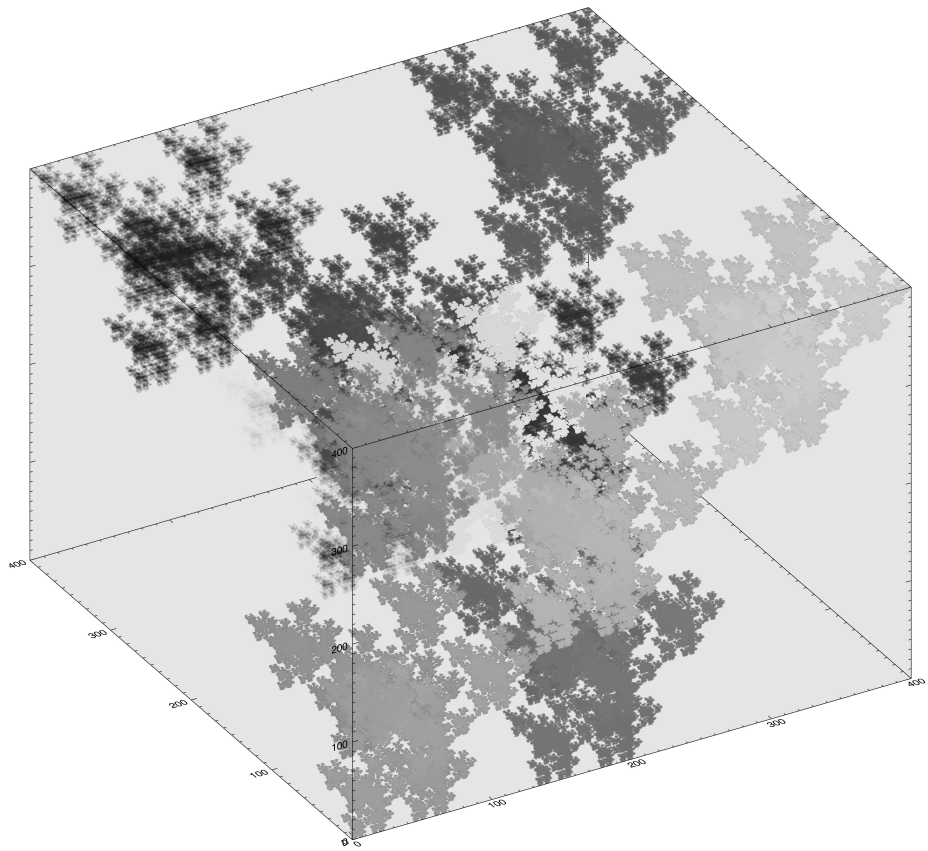

Fig. 3. Volume rendering image of the numerical constructed fractal curve investigated in this study. Grey-levels in the image follow the sequence of calculation in the generation of the fractal from bright to dark — corresponding from early to late in the calculation process. The data was stored in a file in that sequence

We now describe the data reduction method that leads to dissected subsets of the fractal curve. The sequence, within which the points of the fractal curve were calculated, is the sequence within which the xyz-coordinates of the points were written to a list. This sequence contains some information about the geometric neighborhood of a point. We encoded the sequence in grey-levels in Fig. 3 to visualize this. Points at the top of the list are visualized in bright grey-levels, points at the bottom of the list in dark grey-shades. This property of sequence encoded neighborhood information makes it possible to read data from top to bottom direction from the list — up to at maximum $N^6 - 1$ points — to obtain a reduced dissected subset. Again, it is trivial to calculate the number of points needed to represent a reduced set of a certain percent fraction of the complete set, when the set size, N^6, is known by the iteration-level during the construction of the fractal. We generated the following reduced dissected data sets that contain 0.098, 0.195, 0.39, 0.78, 0.83, 1.56, 1.66, 3.13, 6.04, 6.25, 12.5, 13.1, 21.0, 25.0, 28.0, 38.0, 50.0, 67.0, 75.0, 80.0, 90.0, and 96.6 percent points of the complete fractal set.

The method to create reduced eroded subsets of the fractal curve is identical to the method applied for the generation of eroded vessel sets, described earlier. The sequence of the original list of data points of the fractal curve is rigorously shuffled or mixed and stored in a new list. Reduced eroded subsets are generated by reading the points following the sequence of the new list's top to bottom direction — up to the desired set size. Eroded subsets are generated to the same percentage levels as of the dissected subsets shown above.

2.5. Numerical method to estimate the fractal dimension. The method applied to estimate D is the classic "mass radius relation" (mrr) [M, PO, O, SJJ, AL]. The first step in the mrr is to choose an arbitrary point of the set under investigation as a center position c. Next, the number M of "mass-sites", points, or voxels are counted within spheres of radius r, $M(r;c)$. When the structure of interest is a fractal, $M(r;c)$ grows as r^{D_c}:

$$M(r;c) \propto r^{D_c}. \tag{1}$$

The power law in (1) is defined only within a certain range of r values as D_c, which is bounded by an inner and outer cutoff. The inner cutoff $r_{\min}$ is related to the smallest geometrical details in a set. The outer cutoff $r_{\max}$ is related to the largest system size of a set.

The power law (1) defines D_c as a local fractal dimension that is geometrically bounded to the chosen c. We define a global D as the average over many D_c-values, each estimated in an identical scaling range, and each performed from a different, randomly chosen, and not repeating center position of the data set: $D = \langle D_c \rangle$, where $\langle \cdot \rangle$ denotes the average. This ensures that we get a global characterization by D of the irregularity of a set. In this study we have chosen 100 different center positions of each set to estimate D of that set. When we mention D in this study, we always refer to the global fractal dimension, since we are not interested in the local variability of D_c in this investigation.

We implemented the software for the segmentation of the μCT data of the mouse-liver, the fractal curve generation, the programs for the dissection and erosion of the data sets, the visualization of the different sets, and the mrr-method, in the program language IDL® Version 8.1.0, Execlis Visual Information Solutions, Boulder, Colorado, USA.

3. Results. Fig. 4 shows the fractal dimensions results, obtained by the mass radius analysis of the blood vessel system, and of the numerically constructed fractal curve. Both sets were diminished by dissections and erosions to various percent fractions of points of the original data-set size. Fig. 5 shows the differences of $D_{\text{complete set}} - D_{\text{eroded set}}$ and $D_{\text{complete set}} - D_{\text{dissected set}}$ as function of point-set-size reduction in percent of the data shown in Fig. 4.

The results found for minor (preserving roughly up to 80% of points), average (preserving roughly 70 to 10% of points), and major reduction levels (preserving less than approximately 10% of points) are as follows:

For reduction levels that preserve up to approximately 80% of the original set size, we find that a reduction of both sets for both reduction methods has only a marginal effect on the experimentally estimated D, see Figs. 4 and 5.

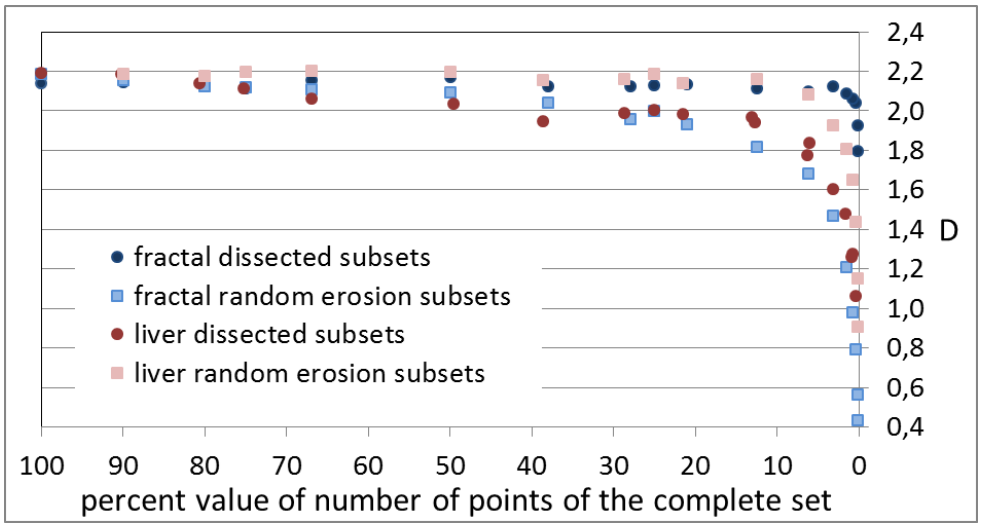

Fig. 4. Results of the numerical D estimates of the four sets described in the graph at various reduction levels

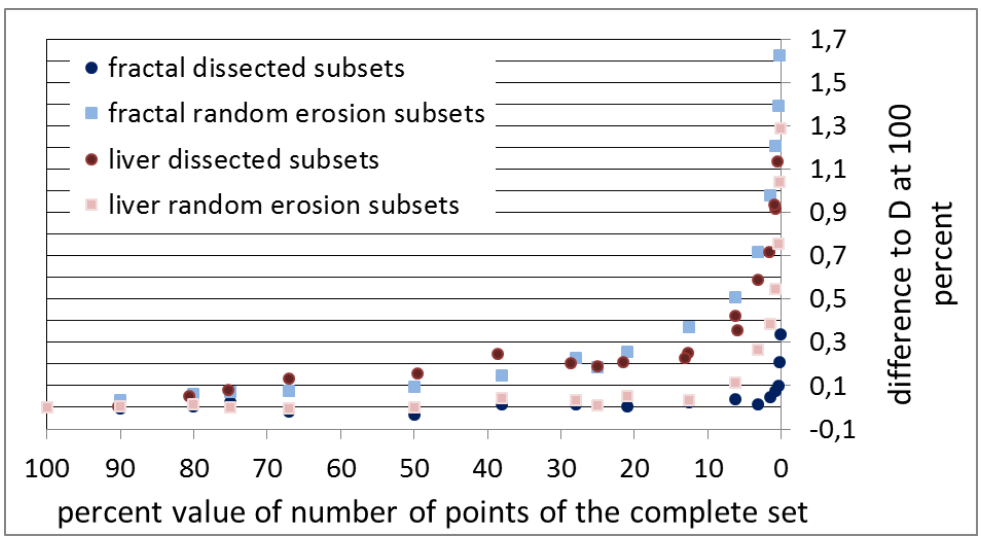

Fig. 5. Differences between D of the original data set and the D at various reduction levels of the four different parameter-variations indicated in the graph

For reduction levels preserving roughly 70 to 10% of the complete set, we find a different behavior of different sets and for the different applied reduction methods: The vessel set, reduced by the erosion method, and the numerical constructed fractal, reduced by the dissection method, retain basically a constant D, even up to reduction levels that preserve only approximately 10% of the original set size. For these sets and for these reduction methods, we find D-deviations between the original set and the reduced set of up to 0.05. Within the same reduction levels from 70 to 10%, the D-deviations between the original set-size and the reduced sets are in a range from 0.1 to 0.4 for the blood

vessel set, reduced by the dissection method, and for the numerically constructed fractal set, reduced by the erosion method.

Reductions that preserve less than approximately 10% of the original set-size, lead to major D-deviations between the original and the reduced set-sizes — for both investigated sets and reduction methods. These D-deviations are numerically estimated up to differences of 1.7. The results in Fig. 4 indicate that both sets for both reduction methods approach D at 0.

4. Discussion

4.1. Minor point size reductions. Figs. 4 and 5 indicate that D remains constant as long as the reduction of the original point set-size retains up to 80%. This is found independent of the investigated set and the applied reduction method. This indicates that the mass radius method is numerically robust. Small set variations, caused e.g. by a minor experimental fluctuation of an imaging technique, should therefore not have a major influence on the numerically obtained D.

4.2. Median point size reductions. The higher reduction rates to smaller point-set-sizes have a different and opposite effect for the vessel system and the numerical constructed fractal curve for both reduction methods.

4.2.1. *Dissection of the blood vessel system.* Reductions caused by dissections of the vessel system, that preserve 70 to 10% of the original set size, lead to variations of D between the original set and the reduced set, of roughly 0.3. This implies that the global geometrical properties, that define the fractal structure, vary for the different dissected vessel subsets. This result has an important implication with respect to the interpretation of D estimates of e.g. a histological biopsy sample. Our finding suggests that D may vary dependent on the position, where the biopsy has been drawn. This can be critical, when the health status of a patient is correlated with D in medical image analysis.

4.2.2. *Dissection of numerical constructed fractal.* Dissections to reductions that preserve only up to 10% of an original data set, allow still a reasonable D estimate of the numerically constructed fractal. This is completely reasonable, since the property of self-similarity means that a fractal preserves its structural properties when it is broken apart into smaller pieces, which is nothing but a dissection. Self-similarity means that the reduction of a fractal to smaller sizes leaves the set invariant. Thus, from the point of view concerning the numerical stability to estimate D, it is interesting to find that this property of self-similarity can be found in numerical experiments up to such large set-size reductions.

4.2.3. *Erosion of the blood vessel system.* Reduced sets obtained by erosions of the vessel set, preserving up to 10% of the complete set size, give a D-estimate that is close to the complete set. This can be explained as follows: The basic fractal property of this set is encoded by the self-similar branching symmetry that is repeated on different length scales. These branches are thick, massive, or fat, which means that the major amount of voxels of the system is contained within a space that can be described by an Euclidean space-filling dimension of 3. An erosion process reduces therefore basically voxels that

reduce the thickness, massiveness, or the fatness of a branch, leaving the global, general geometrical structure invariant. Therefore, this finding is plausible.

4.2.4. *Erosion of numerical constructed fractal.* Reduction of set sizes preserving 70 to 10% of the original set size, which are caused by erosions of the numerically constructed fractal, leads to a decrease of D. This can be understood, since the erosion affects the global geometrical structure. The plot in Fig. 4 suggests a correlation between the number of eroded points and D: The more points are eroded, the smaller gets D. The detailed kind of correlation has to be explored in future numerical experiments.

4.3. Major point size reductions. Reductions of a magnitude such that only 5% or less of points are retained of the original set size, lead to D-values that approach 0. This is reasonable, since the final reduction of all reduction methods leads to a single point of a data set with dimension 0. It is rather remarkable that this is found numerically so late — at reduction levels preserving just 5% of the complete sets.

4.3.1. *General remarks.* The behavior of the different studied influences of data point-size reductions by dissection and by erosion can be plausibly explained for the vessel system and for the numerically constructed fractal. We conclude from these results that fractals can be grouped into different classes by this concept. A "pure" fractal would be the numerically constructed fractal curve, Fig. 3. This set must have the property that a numerical D estimate is invariant under the influence of median range point set-size reductions under dissection. Furthermore, it must have the property that a numerical D estimate varies under the influence of median range point set-size reductions under erosion. An "impure" fractal would have to have the opposite behavior — as found in the example of the vessel system shown in Fig. 2. We assume that this definition of "pure" and "impure" fractals can be used for set differentiations where automated classifications are desired. This would have the advantage of being well-defined, based on algorithms that make human classifications needless.

There are open questions that we shall try to answer in future investigations: What are the statistic results of a detailed analysis of variance including the post hoc tests to differentiate significantly between the four experimental reduced point-size functions: dissected vessel subsets, dissected constructed fractal subsets, eroded vessel subsets, and eroded constructed fractal subsets? The differentiation in minor, average, and major point-size reductions is arbitrarily approached in this study. Are there mathematical models that describe the decrease of D as function of the point-size reduction? They may exist for the erosion method for the pure fractal. They will not exist for the dissection method of the impure fractal. What is a good measure of the variance for the numerical method of the mass radius relation?

The influence of image resolution and noise on the image quality of "pure fractal structures" was studied earlier by Ahammer and colleagues [ADT, AD]. The authors varied e.g. the noise level at a constant number of points of the numerically investigated fractal. They found that increasing levels of noise leads to decreasing D values, which agrees with the findings of this study. No structures that belong into the category of "impure fractals" have been investigated in their study. Other investigations that study the numerical accuracy of fractal dimension estimates are rather focused on box counting

algorithms [AM, KAJ]. Therefore, it might be interesting to compare all the different methods that perform the numerical dimension estimates applied to an even larger variation of different image sets, to obtain a broader overview of the advantages and properties of the numerical methods applied to different image-data types.

5. Conclusion. Many sets of practical relevance in medicine consist of matter with geometrical properties that can be described in parts with Euclidean dimensions, in parts with fractal dimensions. The study of invariance under various degrees of absolute particle size reduction by the two methods — dissection and erosion — seems to enable a numerical definition to classify such different geometry mixture sets. This is most likely of practical relevance for automated system classifications of such sets.

References

[AL] R. Abu Eid, G. Landini, *Quantification of the global and local complexity of the epithelial-connective tissue interface of normal, dysplastic, and neoplastic oral mucosae using digital imaging*, Pathol. Res. Pract. 199 (2003), 475–482.

[AD] H. Ahammer, T. T. J. DeVaney, *The influence of noise on the generalized dimensions*, Chaos Solitons Fractals 26 (2005), 707–717.

[ADT] H. Ahammer, T. T. J. DeVaney, H. A. Tritthart, *How much resolution is enough? Influence of downscaling the pixel resolution of digital images on the generalised dimensions*, Physica D 181 (2003), 147–156.

[AM] H. Ahammer, M. Mayrhofer-Reinhartshuber, *Image pyramids for calculation of the box counting dimension*, Fractals 20 (2012), 281–293.

[KAJ] A. Karperien, H. Ahammer, H. F. Jelinek, *Quantitating the subtleties of microglial morphology with fractal analysis*, Frontiers in Cellular Neuroscience 7 (2013), art. 3.

[M] B. B. Mandelbrot, *The Fractal Geometry of Nature*, Freeman, San Francisco 1982.

[MRR] N. T. Milosević, D. Ristanović, K. Rajković, *Mathematical model of box-counting analysis in the human dentate nucleus during development*, in: Fractals and Complexity, ed. P. Waliszewski, FA Format, Wrocław 2013, ISBN 978-83-936598-0-7, 40–45.

[O] M. Obert, *Numerical estimates of the fractal dimension D and the lacunarity L by the mass radius relation*, Fractals 1 (1993), 711–721.

[PO] P. Pfeifer, M. Obert, *Fractals: Basic concepts and terminology*, in: The Fractal Approach to Heterogeneous Chemistry. Surfaces, Colloids, Polymers, D. Avnir (ed.), J. Wiley & Sons, Chichester 1989, 11–43.

[SJJ] M. Sernetz, M. Justen, F. Jestczemski, *Dispersive fractal characterization of kidney arteries by three-dimensional mass-radius-analysis*, Fractals 3 (1995), 879–891.

[S] W. Sierpiński, *Sur une courbe dont tout point est un point de ramification*, C. R. Acad. Sci. 160 (1915), 302–305.